Check for updates

LASER & PHOTONICS REVIEWS
www.lpr-journal.org

1 PHz of Coherent Bandwidth from a Compact Fiber Device

*Sarah R. Hutter, Philipp Sterk, Sarah Haller, Moritz Cimander, and Alfred Leitenstorfer**

Femtosecond frequency combs uniquely combine high frequency resolution, wide spectral coverage, and the ability to generate single-cycle pulses, rendering them essential for fundamental research and applied photonics. However, effective dispersion management across vast bandwidths remains a major challenge, often requiring complex setups that compromise stability and efficiency. Here, a coherent comb spectrum is presented with an unprecedented bandwidth of 1 PHz, spanning from the deep ultraviolet (280 nm) to the mid-infrared (2700 nm). This output is generated by a compact fiber device pumped by an ultrastable Er:fiber system. By integrating two highly nonlinear fibers with distinct germanium doping and waveguide design, a flat dispersion profile is achieved across the entire mid- and near-infrared spectral region. This pulse purification technology facilitates efficient third-harmonic generation within the same nonlinear device enabling the synthesis of ultrashort pulses with an exceptionally clean temporal envelope. Using a novel spectral filter and customized chirped mirrors, single-cycle near-infrared pulses with a duration of 3.56 fs are obtained. Beat signals between the fundamental dispersive wave and its third harmonic exhibit exceptional long-term passive stability, underpinning the reliability of this concept. This compact and versatile approach marks a significant leap forward in the generation and control of coherent supercontinua.

1. Introduction

Broadband coherent light sources represent powerful tools in modern physics, driving significant advances in both scientific and industrial settings. Supercontinuum-based spectroscopy,[1] for example, offers unmatched precision and sensitivity, enabling detailed analysis of molecular structures[2] and chemical bonds.[3] In biomedicine, emitters with a high spectral bandwidth are vital for non-invasive imaging techniques,[4] and in climate science, they allow real-time monitoring of environmental conditions.[5] Additionally, these sources are essential for fast, reliable data transmission.[6] In this context, optical frequency combs[7,8] are uniquely capable of generating broadband electromagnetic radiation across the visible,[9,10] near-infrared (NIR),[11,12] and mid-infrared (MIR) spectral regions,[13,14] while simultaneously ranking amongst the most precise measurement tools available. Such instruments are indispensable for high-precision timekeeping and frequency metrology,[15] pushing the limits in optical clock technology[16] to redefine fundamental constants with unprecedented precision.[17] Femtosecond mode-locked lasers form the heart of these systems, typically operating in the NIR.[12] To significantly expand their spectral coverage, methods relying on nonlinear optical processes have been established which are generally classified into two categories: frequency upconversion via high-order harmonics[18,19] and supercontinuum generation in waveguides[9,20–23] or special fibers,[24] including liquid-core,[25] photonic crystal,[26] and highly nonlinear fibers.[27] Accessing the high-frequency part of the electromagnetic spectrum is crucial, e.g. for advanced concepts in quantum computing and simulation[28,29] – a rapidly evolving field that demands reliable and precise light sources in the visible and ultraviolet (UV) for effective manipulation and detection of atomic or molecular quantum states. Motivated by this need, significant progress has been made to extend comb coverage even into the UV.[9,10,19]

Still, methods to broaden the output spectrum of a femtosecond laser often rely on complex systems, which are inherently prone to noise and lack long-term stability. Furthermore, most approaches target one frequency region and cannot provide smooth spectral coverage across several hundreds of THz. Here, we present a femtosecond frequency comb with a bandwidth of 1 Petahertz (1 PHz = 10^{15} Hz) providing equidistant, coherent spectral lines in the ultraviolet, visible, near-infrared, and mid-infrared regions. This extreme supercontinuum is generated via $\chi^{(3)}$ processes in a nonlinear fiber assembly seeded by a compact femtosecond Er:fiber laser. By combining two tailored types of solid-core germanosilicate fibers, we achieve a flat dispersion profile across the entire mid- and near-infrared parts of the ultrabroadband spectrum. The resulting single-cycle pulses feature an exceptionally clean temporal envelope and high intensities. These characteristics enable efficient third harmonic generation (THG) directly within the fiber device, thereby extending

S. R. Hutter, P. Sterk, S. Haller, M. Cimander, A. Leitenstorfer
Department of Physics and Center for Applied Photonics
University of Konstanz
78457 Konstanz, Germany
E-mail: alfred.leitenstorfer@uni-konstanz.de

The ORCID identification number(s) for the author(s) of this article can be found under https://doi.org/10.1002/lpor.202500355

© 2025 The Author(s). Laser & Photonics Reviews published by Wiley-VCH GmbH. This is an open access article under the terms of the Creative Commons Attribution License, which permits use, distribution and reproduction in any medium, provided the original work is properly cited.

DOI: 10.1002/lpor.202500355

Konstanzer Online-Publikations-System (KOPS)
URL: http://nbn-resolving.de/urn:nbn:de:bsz:352-2-ce1n5g9267er4

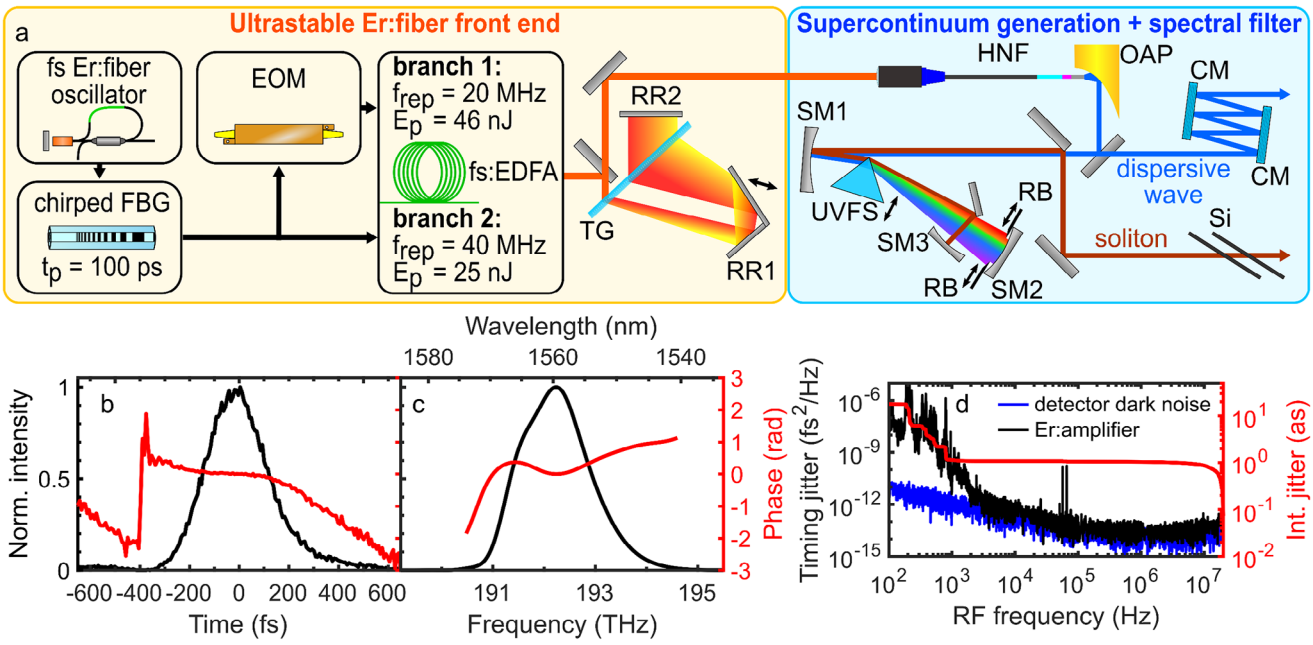

Figure 1. Overview of experimental setup for hyperbroadband continuum generation. a) Sketch of low-noise Er:fiber laser system with dual branches (yellow box) and subsequent setup for extreme spectral broadening (blue box). The pulses emitted from the mode-locked Er:fiber oscillator are stretched to 100 ps via a chirped fiber Bragg grating (FBG) and then split into two paths. Both arms are designed similarly, with branch 1 including a fiber-coupled electro-optic modulator (EOM) to reduce the repetition rate to 20 MHz. A femtosecond Er:fiber amplifier (fs:EDFA) boosts the pulse energies, followed by temporal compression using a single transmission grating (TG). The hyperbroadband continuum is generated in a highly nonlinear fiber (HNF) assembly and spectrally filtered using a UV-grade fused silica (UVFS) prism and three spherical mirrors (SM1-SM3). Their focal lengths are f_1 = 250 mm and $f_2 = f_3$ =100 mm. Two customized chirped mirrors (CMs) compensate the dispersion introduced by the prism. RR: retroreflector; RB: razor blade; OAP: off-axis parabola; Si: silicon wafer. b) Temporal and c) spectral intensity (black) and corresponding phase (red) of the pulses after the grating compressor. d) Timing jitter power spectral density (black) and integrated rms timing jitter (red).

the spectral comb coverage smoothly and continuously across the entire visible and significantly into the UV. In contrast to approaches based on lithium niobate waveguides[9,10,30] which are limited by a direct bandgap at 4 eV, corresponding to a frequency of 967 THz, our concept demonstrates generation of coherent radiation up to 1070 THz (wavelength of 280 nm). The emergence of beat signals between the fundamental dispersive wave and the third harmonic verifies the optical coherence and serves to demonstrate the excellent long-term stability of our concept. This unparalleled bandwidth provided by a compact approach, combined with the resulting clean, ultrashort pulses unlocks new opportunities for high-precision applications in both the frequency and time domains.

2. Results and Discussion

2.1. Experimental Setup

The key aspects of our experiment are illustrated in **Figure 1a**. The setup consists of two main parts: an ultrastable Er:fiber front end with dual branches (yellow box) and two modules for generating a hyperbroadband continuum, followed by spectral filtering (blue box). The core of our low-noise laser system is a femtosecond Er:fiber oscillator based on a nonlinear amplifying loop mirror.[31–34] Through additive-pulse mode-locking,[35–37] it produces a frequency comb with a repetition rate of 40 MHz. By precisely engineering the intracavity dispersion, we achieve linewidths below 3 kHz across the entire spectrum from the carrier-envelope offset (CEO) frequency up to 300 THz.[34] After the oscillator, the output pulses are temporally stretched from 100 fs to 100 ps using a chirped fiber Bragg grating (FBG) and subsequently divided into two separate branches. While one is kept at 40 MHz, an electro-optic modulator (EOM) reduces the repetition rate to 20 MHz in the other branch, enabling ultra-sensitive pump-probe experiments with high-frequency lock-in detection. This compact, fully fiber-integrated pulse picking scheme facilitates the generation of any subharmonic of the oscillator repetition rate without introducing additional intensity or phase noise to the pulse train.

Both branches 1 and 2 feature core-pumped Erbium-doped fiber amplifiers (EDFAs), boosting pulse energies to 46 and 25 nJ, respectively. Up to this point, the entire system is constructed using only polarization-maintaining fiber components, which are readily available from telecom industry, cost-effective, and enhance stability as well as compactness. Only now, the amplified pulses are coupled into free space, where they undergo temporal compression in a grating compressor composed of a single transmission grating (TG) and a horizontal (RR1) and vertical retroreflector (RR2). The dielectric grating (Gitterwerk GmbH) on a 3 mm thick ultra-pure fused silica substrate has a line density of 800 l/mm and a transmission efficiency of >99% across a 100-nm bandwidth centered at 1550 nm. Together with

© 2025 The Author(s). Laser & Photonics Reviews published by Wiley-VCH GmbH

the dielectrically coated mirrors, this design achieves over 94% overall transmission efficiency while minimizing alignment errors. By placing RR1 on a linear translation stage, we can fine-tune the total dispersion. The recompressed pulses are characterized using second-harmonic generation frequency-resolved optical gating[38] and an optical spectrum analyzer. Figure 1b,c presents the resulting temporal and spectral intensity (black) along with the corresponding phase (red). Since the dispersion of the FBG and the grating compressor are carefully aligned up to fourth order, nearly flat phase characteristics are achieved, resulting in a clean temporal pulse shape. The chirped-pulse amplification concept[39,40] enables high gain while avoiding the challenges posed by nonlinear effects. Moreover, the amplifier reduces the spectral bandwidth due to gain narrowing, effectively suppressing sidebands that are highly susceptible to pump noise.[41]

To emphasize the extraordinary stability of our system, we characterize the timing jitter of the pulse train after the grating compressor with a method based on interferometric cross-correlation between subsequent pulses (see Section S1, Supporting Information). Figure 1d shows the respective noise spectral density, which is primarily influenced by acoustic resonances up to 2 kHz. Beyond this range, the signal is merely above the dark noise of the photodetector. The root-mean-square (rms) timing jitter (red) indicates an upper limit of 1 attosecond when integrated from 2 kHz up to the Nyquist frequency $f_{\mathrm{Ny}} = 20$ MHz. To the best of our knowledge, this represents the lowest value ever measured for a fiber-based femtosecond laser. Even with 100 Hz as the lower integration limit, the rms timing jitter approaches merely 20 as.

These intense, low-noise 280-fs-pulses are an ideal starting point for significantly extending the spectral comb coverage. The innovative setup for supercontinuum generation and spectral filtering is identical in both branches and displayed in the blue box in Figure 1a. First, an ultrabroadband spectrum is generated via extreme third-order processes in a highly nonlinear fiber (HNF) assembly. Next, a dispersive Fourier filter based on a UV fused silica (UVFS) Brewster prism and three spherical mirrors (SM1-SM3) spatially separates the wavelengths. Two razor blades (RB) in the Fourier plane of SM1 enable precise selection of the high-frequency dispersive wave (blue), which is reflected back with a slight vertical offset by SM2. To compensate for the dispersion introduced by the prism, we employ a pair of customized chirped mirrors (CMs, Laseroptik GmbH). The combined reflection from both mirrors accurately cancels out the material dispersion of 3 mm UVFS between 700 and 1400 nm while providing a reflection efficiency of more than 99%. Moving the prism in and out of the beam path provides a degree of freedom for fine-tuning the overall dispersion. By increasing the number of bounces on the CMs, the impact of additional UVFS transmissive optical elements, such as cryostat windows, may also be balanced out. Due to their strong temporal distortion, the fundamental components ≈1550 nm are discarded. The low-frequency soliton (brown) is isolated by a pickoff mirror placed in front of the razor blades and sent back by an additional spherical mirror (SM3) with a slightly different vertical offset. Long focal lengths of the spherical mirrors allow very small vertical beam angles, ensuring that spatial chirp remains negligible. In the solitonic beam path, two 500-µm-thick silicon (Si) wafers inserted under Brewster's angle compensate for the anomalous dispersion of the UVFS prism.

2.2. Nonlinear Fiber Device with Ultrabroadband Dispersion Engineering

Building on the general overview of our experimental setup, this section delves into the highly nonlinear fiber assembly enabling generation of an extreme supercontinuum. To overcome the challenges of achieving a flat phase after spectral broadening, we developed a compact and robust device that directly incorporates ultrabroadband dispersion engineering. To this end, mature Er:fiber technology offers two significant advantages: first, full compatibility with standard telecom components such as free-space couplers (FSCs), which provide a coupling efficiency above 80% along with excellent long-term stability. More importantly, light emission at 1550 nm (193 THz) supports extreme four-wave mixing processes in germanosilicate fibers, which exhibit a zero-crossing of the group velocity dispersion around a wavelength of 1400 nm (214 THz). Commercially available solid-core fibers differ in Ge doping and waveguide dispersion, which are the key parameters that determine their dispersion characteristics and optical nonlinearity. **Figure** 2a presents the group delay dispersion (GDD) of two germanosilicate fibers as obtained by white-light interferometry. HNF1 (cyan line, HNLF 072649860005 from OFS) has a core diameter of 4 µm and a nonlinearity of 9 kW^{-1} whereas HNF2 (pink graph, GF3 from Nufern) features a core diameter of 7 µm and a nonlinearity of 2.7 kW^{-1}. The combination of these carefully selected pieces yields an exceptionally flat overall dispersion profile (black line), representing the cornerstone of our innovative pulse purification technology. Using standard fusion splicing, the two HNFs can be easily integrated with an FSC and a short segment of coreless fiber. The latter acts as an endcap (EC) to adiabatically increase the mode field diameter, ensuring long-term stability. The inset in Figure 2b provides an overview of the entire fiber assembly.

Propagation within the first section is predominantly governed by self-phase modulation. As a result, the pulses undergo spectral broadening and split up into two components: a high-frequency dispersive wave and a soliton at longer wavelengths. Both parts maintain temporal overlap in the subsequent germanosilicate fibers due to the zero-crossing of the GDD around a wavelength of 1400 nm. This feature facilitates efficient four-wave mixing processes, substantially enhancing the optical bandwidth. As discussed later, the integrated pulse purification technique produces ultraclean pulses with optimum peak intensities. Owing to the large phase mismatch in the visible and UV, this fact is crucial for efficient generation of the third harmonic within the very last section of the highly nonlinear device before emission into the coreless endcap. As a consequence, a hyperbroadband spectrum results spanning seamlessly over more than three octaves with a total bandwidth of 1 PHz (Figure 2b). Without additional conversion steps, we achieve frequency comb coverage in the ultraviolet, visible, near-infrared, and mid-infrared spectral region. The soliton contains an average power of 200 mW, corresponding to an average of 50 nW per comb tooth assuming a flat spectrum. The dispersive wave reaches 55 mW (5 nW per comb tooth) and 1 mW (0.1 nW per mode) is delivered in the visible. 4 µW (0.25 pW per mode) are transferred to the UV below 400 nm. This extensive bandwidth establishes our device as an efficient and versatile white-light source (see photograph in Figure 2b), suitable for a wide variety of applications.

© 2025 The Author(s). Laser & Photonics Reviews published by Wiley-VCH GmbH

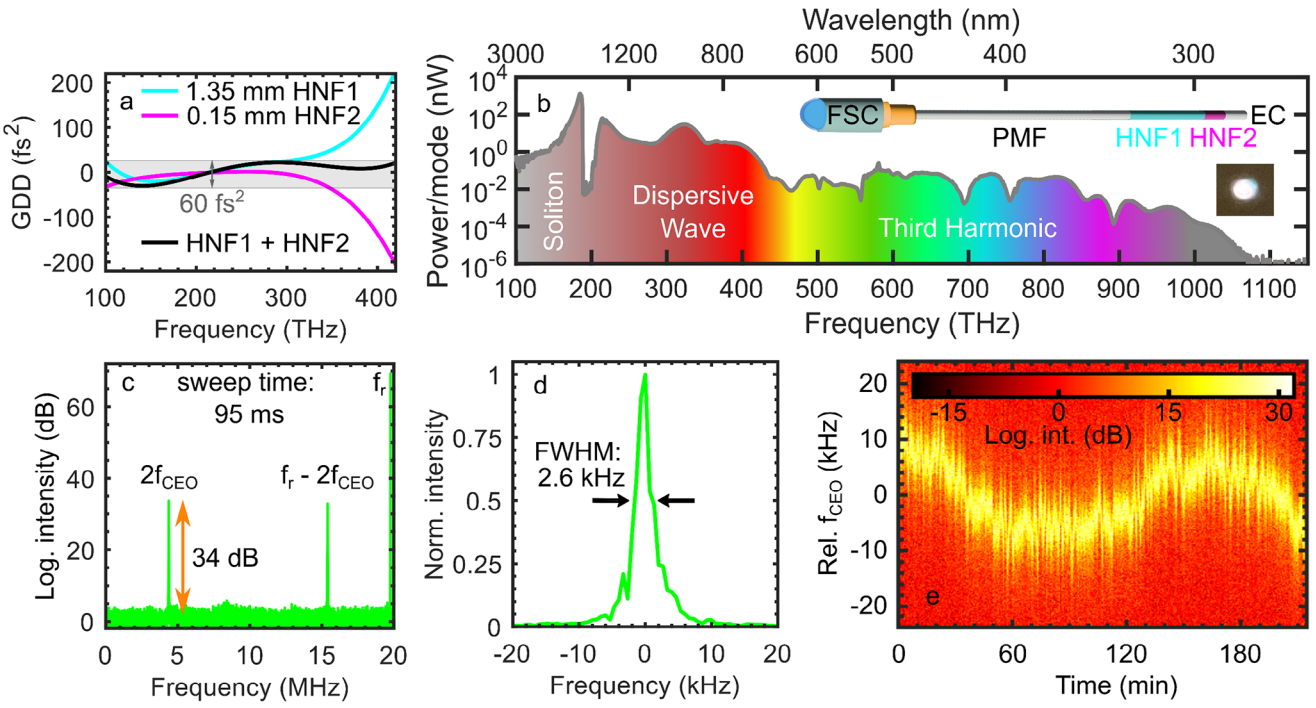

Figure 2. 1 PHz coherent spectrum and resulting facilities. a) Ultrabroadband dispersion profiles of two highly nonlinear germanosilicate fibers (HNF1 and HNF2), as measured via white-light interferometry. The cyan, pink, and black lines represent the group delay dispersion (GDD) of 1.35 mm HNF1, 0.15 mm HNF2, and the combination of both, respectively. The resulting GDD remains minimum and within a margin as narrow as 60 fs^2 from 100 to 420 THz (gray band and arrows). b) Hyperbroadband supercontinuum generated by the customized nonlinear fiber device featuring ultrabroadband dispersion control. The fiber assembly (inset) includes a free-space coupler (FSC), a polarization-maintaining telecom fiber (PMF), two highly nonlinear germanosilicate fibers (HNF1 and HNF2), and an endcap (EC). The resulting spectrum spans from 110 THz (2700 nm) to 1.07 PHz (280 nm). The photograph captures the resulting white light. c) RF spectrum showing the beat signals emerging due to the interference between the fundamental dispersive wave and the third harmonic (500 Hz resolution bandwidth, 20 Hz video bandwidth). d) Spectral width of the beat signal centered at $2f_{CEO}$. e) Long-term stability of the free-running carrier-envelope offset frequency f_{CEO}.

Since the fundamental dispersive wave and the third harmonic overlap spectrally, they can interfere and provide access to the carrier-envelope offset frequency of the comb. By measuring the light emerging from the fiber device with a standard photodetector, we observe beat notes at $2f_{CEO}$ and f_r-$2f_{CEO}$. This finding confirms the optical coherence of the supercontinuum and attributes the high-frequency spectral components to THG. While the characteristic peaks are readily observable on top of the entire optical bandwidth, we enhance the signal-to-noise ratio to 34 dB by employing the dispersive Fourier filter presented in Figure 1a. The two razor blades are used to precisely select the spectral region from 550 to 700 nm, which contains the beat signals. The resulting RF spectrum is depicted in Figure 2c. It is exceptionally clean with the emerging signals exhibiting a full width at half maximum (FWHM) as small as 2.6 kHz (Figure 2d, measurement time: 95 ms). To demonstrate the long-term stability of our concept, we track the intensity and position of the beat notes for over 3.5 h. As shown in Figure 2e, the CEO frequency drifts only by 20 kHz during this period without active feedback. This finding underlines the excellent thermal stability of our compact oscillator, which is easily stabilized to 296 K ± 2 mK even under standard laboratory conditions. In addition, the signal-to-noise ratio remains constant throughout the measurement, emphasizing the stability of the spectral parts that generate the beat signals. Combined with its high coupling efficiency and robustness, our nonlinear fiber device is ideally suited for carrier-envelope phase stabilization.

Our pulse purification approach significantly extends the spectral comb coverage and refines the temporal shape of the resulting pulses. To illustrate the benefits in the frequency and time domain, we perform numerical simulations. The pulse propagation within the fiber assembly is modeled using a generalized nonlinear Schrödinger equation that is solved via a symmetric split-step Fourier scheme. **Figure 3**a shows the simulated output spectra of the dispersive wave after propagation through 10.70 cm of polarization-maintaining telecom fiber (PMF) and 1.35 mm of HNF1 (blue graph), compared to the scenario with an additional 0.15 mm of HNF2 (red curve). While the spectral energy distribution of the dispersive wave changes only slightly, the spectral phase (red-dashed line) exhibits notable flattening. This reduction of higher-order dispersion is also evident in the experimental data. The gray area represents the measured output spectrum, accompanied by the corresponding phase (black-dashed line), as obtained by 2D spectral shearing interferometry (2DSI; see Section S2, Supporting Information).[42] Figure 3b presents the temporal intensity derived from simulations (red and blue lines) alongside the experimental data (black graph). The combination of two tailor-selected HNFs significantly suppresses satellite pulses, concentrating the energy into a single peak. Our broadband dispersion control boosts the intensity by 25%, result-

© 2025 The Author(s). Laser & Photonics Reviews published by Wiley-VCH GmbH

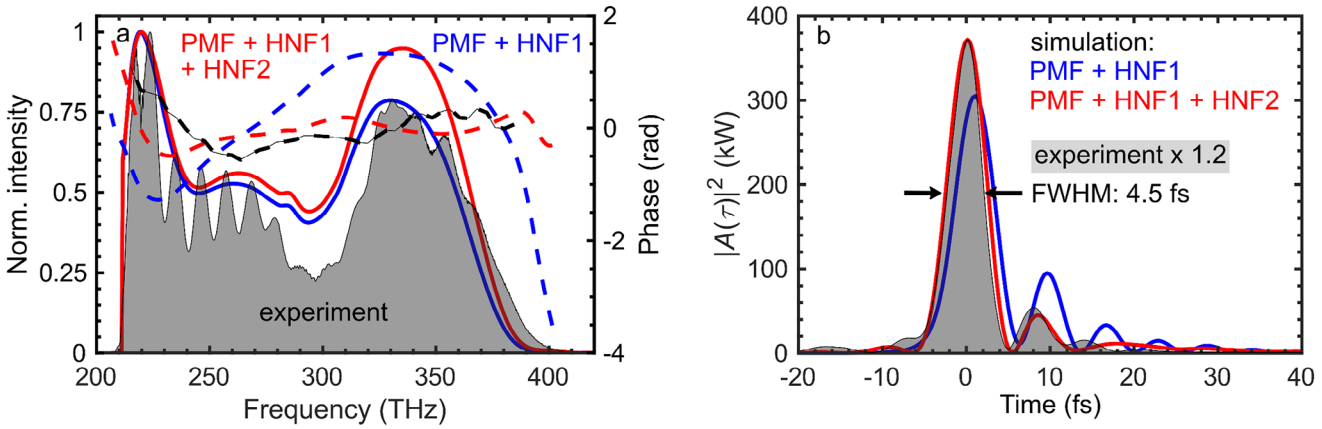

Figure 3. Pulse Purification Technology based on ultrabroadband dispersion control. a) Infrared output spectrum of the nonlinear fiber device and corresponding spectral phase (dashed) versus frequency. The blue and red lines represent the spectral characteristics obtained via simulations for a fiber assembly comprising a polarization-maintaining fiber (PMF) with one or two highly nonlinear germanosilicate fibers (HNFs), respectively. The black graph indicates the measured output spectrum emerging from the nonlinear fiber device introduced in Figure 2, while the dashed line highlights the reconstructed phase. b) Temporal intensity profiles derived from simulations (blue and red curve) and the Fourier transform of the 2DSI data (black graph), as measured after the dispersive Fourier filter and the chirped mirrors. The experimental data is scaled with a factor of 1.2 to account for additional losses.

ing in 4.5-fs-pulses with over 80% of the total energy confined to the main peak. These high peak intensities drive efficient third harmonic generation in the final section of the fiber device, significantly extending the frequency comb spectrum into the ultraviolet. The strong agreement between measurement and simulation underscores the accuracy and versatility of our model. In addition to accurately predicting the temporal shape, the model reliably estimates the absolute power of the dispersive wave. The remaining 20% discrepancy can be attributed to additional losses occurring at the splices and output facet. Our ultrabroadband dispersion control refines the temporal pulse shape, thereby improving the excitation efficiency and increasing the signal brightness, which enhances performance in applications such as two-photon microscopy.[43]

2.3. Single-Cycle Near-Infrared Pulse

Using solely the dispersive wave, we achieve pulse durations as short as 4.5 fs, corresponding to less than 1.5 optical cycles at a center frequency of 315 THz. However, the synthesis of single-cycle pulses becomes feasible by additionally leveraging the low-frequency soliton. To recombine the two spatially separated components, both are focused into the nonlinear crystal of the 2DSI setup. A delay stage in the beam path of the soliton ensures temporal overlap between the two arms (see Section S2, Supporting Information for details). **Figure** 4a depicts the measured spectra of the dispersive wave (cyan) and the solitonic part (brown), along with the spectral phase (red). Our pulse purification technology ensures an exceptionally flat dispersion across a bandwidth exceeding 300 THz. Only the soliton exhibits residual third-order dispersion from propagation through the UVFS prism, which is not fully compensated by the two silicon wafers. Nevertheless, a Fourier transform of the complete spectrum and phase yields a pulse with a FWHM duration of 3.56 fs (Figure 4b), corresponding to a single optical cycle at the center frequency of 280 THz. Temporal side maxima remain below 20% of the peak pulse intensity. The high efficiency of our setup allows for a total pulse energy of 3.8 nJ, with 49% concentrated in the main peak. Figure 4c shows the normalized electric field of the pulse assuming a cosine-like carrier-envelope phase. A significant asymmetry is observed between the central positive and adjacent negative field extrema, with the negative ones reaching only 70% of the maximum field strength, rendering our system ideal for advanced applications like e.g., petahertz electronics[44] as well as integrated and nonperturbative nonlinear optics.[45,46]

3. Summary and Conclusion

Ultrabroadband frequency combs are powerful instruments, offering equidistant spectral lines across wide optical bandwidths. Nevertheless, achieving smooth spectra and dispersion over several octaves remains a challenge, often requiring complex and bulky systems that are prone to pick-up noise. This work addresses these issues presenting a compact and robust nonlinear fiber device with integrated high-order dispersion management. We show that by combining two germanosilicate fibers, it is possible to obtain a flat spectral phase over more than 300 THz. This innovation produces pulses with high peak intensities, enabling efficient third-harmonic generation directly within the fiber assembly. Our pulse purification technology delivers a smooth 1-PHz continuum spanning from 280 to 2700 nm, offering sharp comb lines in the ultraviolet, visible, near- and mid-infrared regions. Emerging f-3f beat notes confirm the optical coherence and demonstrate the excellent long-term stability of our concept. A compact spectral filtering setup offers precise tailoring of the ultrabroadband spectrum without introducing dispersion.

Our approach combines an unprecedented bandwidth with long-term reliability and low noise, establishing new standards for the spectral coverage femtosecond frequency combs can directly provide. Owing to the versatility of the concept, it is compatible with systems operating at a wide range of repetition rates,

© 2025 The Author(s). Laser & Photonics Reviews published by Wiley-VCH GmbH

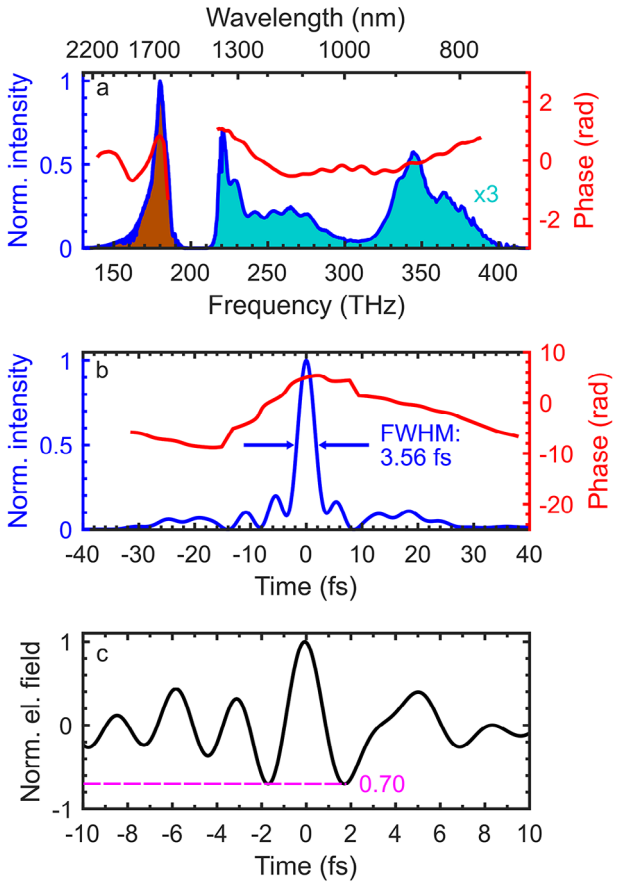

Figure 4. Spectral and temporal characterization of single-cycle pulses. a) Spectral intensity of the soliton (brown) and dispersive wave (cyan, scaled by a factor of 3), as measured by two optical spectrum analyzers. The complete spectral phase (red) is obtained via 2D spectral shearing interferometry. b) Temporal intensity (blue) and corresponding phase (red), derived from the Fourier transform of the spectrum and phase information in (a). The full width at half maximum (FWHM) pulse duration is 3.56 fs. c) Normalized electric field of the single-cycle pulses for a cosine-like phase. The pink-dashed line highlights the asymmetry between the center positive and the adjacent negative half-cycles.

including the GHz regime, provided that the front-end source delivers sufficient pulse energy. Its vast applicability ranges from ultrabroadband pump-probe-experiments and atomic clock technology to the precise control of quantum systems. The new pulse purification technology refines the temporal envelope of the resulting single-cycle pulses, significantly enhancing their potential for ambitious tasks in ultrafast physics.[45–49] Supported by simulations, our findings may be reproduced easily. Therefore, they are compatible with a wide range of femtosecond laser systems, offering a versatile platform for advanced applications in the frequency and time domains.

Supporting Information

Supporting Information is available from the Wiley Online Library or from the author.

Acknowledgements

Funding: This work was funded by the Deutsche Forschungsgemeinschaft (DFG, German Research Foundation) - SFB 1432 - Project-ID 425217212.
Open access funding enabled and organized by Projekt DEAL.

Conflict of Interest

The authors declare no conflict of interest.

Author Contributions

S.R.H. and P.S. contributed equally to this work. S.R.H., P.S., S.H., and M.C. carried out the experiments. S.R.H., P.S., S.H., and A.L. analyzed the data. A.L. initiated the project and supervised the work. S.R.H., P.S., and A.L. wrote, and all authors commented on the manuscript.

Data Availability Statement

The data that support the findings of this study are available from the corresponding author upon reasonable request.

Keywords

femtosecond frequency combs, fiber lasers, nonlinear optics, supercontinuum generation, ultrafast optics, ultralow noise

Received: February 17, 2025
Revised: May 13, 2025
Published online: May 28, 2025

[1] I. Coddington, N. Newbury, W. Swann, *Optica* **2016**, *3*, 414.
[2] S. A. Diddams, L. Hollberg, V. Mbele, *Nature* **2007**, *445*, 627.
[3] A. H. Zewail, *J. Phys. Chem. A* **2000**, *104*, 5660.
[4] C. Poudel, C. F. Kaminski, *J. Opt. Soc. Am. B* **2019**, *36*, 139.
[5] C. F. Kaminski, R. S. Watt, A. D. Elder, J. H. Frank, J. Hult, *Appl. Phys. B* **2008**, *92*, 367.
[6] Y V. Grachev, X. Liu, S E. Putilin, A N. Tsypkin, V G. Bespalov, S A. Kozlov, Xi-C Zhang, *IEEE Photonics Technol. Lett.* **2018**, *30*, 103.
[7] J. L. Hall, *Rev. Mod. Phys.* **2006**, *78*, 1279.
[8] T. W. Hänsch, *Rev. Mod. Phys.* **2006**, *78*, 1297.
[9] T. H. Wu, L. Ledezma, C. Fredrick, P. Sekhar, R. Sekine, Q. Guo, R. Briggs, A. Marandi, S. Diddams, *Nat. Photonics* **2024**, *18*, 218.
[10] J. Rutledge, A. Catanese, D. D. Hickstein, S. A. Diddams, T. K. Allison, A. S. Kowligy, *J. Opt. Soc. Am. B* **2021**, *38*, 2252.
[11] A. L. Gaeta, M. Lipson, T. J. Kippenberg, *Nat. Photonics* **2019**, *13*, 158.
[12] S. A. Diddams, K. Vahala, T. Udem, *Science* **2020**, *369*, aay3676.
[13] A. Schliesser, N. Picqué, T. W. Hänsch, *Nat. Photonics* **2012**, *6*, 440.
[14] A. Roy, L. Ledezma, L. Costa, R. Gray, R. Sekine, Q. Guo, M. Liu, R. Briggs, A. Marandi, *Nat. Commun.* **2023**, *14*, 1.
[15] D. J. Jones, S. Diddams, J. Ranka, et al., *Science* **2000**, *288*, 130.
[16] A. D. Ludlow, M. M. Boyd, J. Ye, E. Peik, P. O. Schmid, *Rev. Mod. Phys.* **2015**, *87*, 637.
[17] J. M. Robinson, M. Miklos, Y. Tso, C. Kennedy, T. Bothwell, D. Kedar, J. Thompson, J. Ye, *Nat. Phys.* **2024**, *20*, 208.
[18] J. J. Macklin, J. D. Kmetec, C. L. Gordon, *Phys. Rev. Lett.* **1993**, *70*, 766.
[19] I. Pupeza, C. Zhang, M. Högner, J. Ye, *Nat. Photonics* **2021**, *15*, 175.
[20] M. W. Pruessner, N. F. Tyndall, J. B. Khurgin, W. S. Rabinovich, P. G. Goetz, T. H. Stievater, *Nat. Commun.* **2024**, *15*, 1.

© 2025 The Author(s). Laser & Photonics Reviews published by Wiley-VCH GmbH

[21] M. R Escalé, F. Kaufmann, H. Jiang, D. Pohl, R. Grange, *APL Photon.* **2020**, *5*, 1.
[22] Y. Fang, C. Bao, S. Li, Z. Wang, W. Geng, Y. Wang, X. Han, J. Jiang, W. Zhang, Z. Pan, Z. Li, Y. Yue, *Laser Photon Rev* **2023**, *17*, 1.
[23] A. Ishizawa, K. Kawashima, R. Kou, X. Xuejung, T. Tsuchizawa, T. Aihara, K. Yoshida, T. Nishikawa, K. Hitachi, G. Cong, N. Yamamoto, K. Yamada, K. Oguri, *Opt. Express* **2022**, *30*, 5265.
[24] T. Sylvestre, E. Genier, A. Ghosh, P. Bowen, G. Genty, J. Troles, A. Mussot, A. Peacock, M. Klimczak, A. Heidt, J. Travers, O. Bang, J. Dudley, *J. Opt. Soc. Am. B* **2021**, *38*, 90.
[25] R. Scheibinger, N. Lüpken, M. Chemnitz, K. Schaarschmidt, J. Kobelke, C. Fallnich, M. Schmidt, *Sci. Rep.* **2021**, *11*, 1.
[26] J. M. Dudley, G. Genty, S. Coen, *Rev. Mod. Phys.* **2006**, *78*, 1135.
[27] D. Brida, G. Krauss, A. Sell, A. Leitenstorfer, *Laser Photon Rev.* **2014**, *8*, 409.
[28] T. D. Ladd, F. Jelezko, R. Laflamme, Y. Nakamura, C. Monroe, J. L. O'Brien, *Nature* **2010**, *464*, 45.
[29] H. Häffner, C. F. Roos, R. Blatt, *Phys. Rep.* **2008**, *469*, 155.
[30] K. Iwakuni, S. Okubo, O. Tadanaga, H. Inaba, A. Onae, F. Hong, H. Sasada, *Opt. Lett.* **2016**, *41*, 3980.
[31] M. E. Fermann, F. Haberl, M. Hofer, H. Hochreiter, *Opt. Lett.* **1990**, *15*, 752.
[32] N. Kuse, J. Jiang, C. Lee, T. Schibli, M. Fermann, S. Diddams, D. Jones, J. Ye, S. Cundiff, J. Hall, J. Ranka, R. Windeler, R. Holzwarth, T. Udem, T. Hänsch, D. Yost, M. Martin, A. Marcinkevicius, M. Fermann, *Opt. Express* **2016**, *24*, 3095.
[33] T. Jiang, Y. Cui, P. Lu, C. Li, A. Wang, Z. Zhang, *IEEE Photonics Technol. Lett.* **2016**, *28*, 1786.
[34] S. R. Hutter, A. Seer, T. König, R. Herda, D. Hertzsch, H. Kempf, R. Wilk, A. Leitenstorfer, *Laser Photon Rev.* **2023**, *17*, 2200907.
[35] E. P. Ippen, H. A. Haus, L. Y. Liu, *J. Opt. Soc. Am. B* **1989**, *6*, 1736.
[36] E. P. Ippen, J. G. Fujimoto, H. A. Haus, *J. Opt. Soc. Am. B* **1991**, *8*, 2068.
[37] H. A. Haus, K. Tamura, L. E. Nelson, E. P. Ippen, *IEEE J. Quantum Electron.* **1995**, *31*, 591.
[38] K. W. DeLong, J. Hunter, R. Trebino, W. E. White, *J. Opt. Soc. Am. B* **1994**, *11*, 2206.
[39] G. Mourou, *Rev. Mod. Phys.* **2019**, *91*, 030501.
[40] D. Strickl, *Rev. Mod. Phys.* **2019**, *91*, 30502.
[41] C. Wan, T. Schibli, P. Li, C. Bevilaqua, A. Ruehl, I. Hartl, *Opt. Lett.* **2017**, *42*, 5266.
[42] J. R. Birge, F. X. Kärtner, R. Ell, *Opt. Lett.* **2006**, *31*, 2063.
[43] S. P. Chong, P. Török, *Opt. Contin.* **2024**, *3*, 552.
[44] T. Rybka, M. Ludwig, M. F. Schmalz, V. Knittel, D. Brida, A. Leitenstorfer, *Nat. Photonics* **2016**, *10*, 667.
[45] S. Meier, J. Heimerl, P. Hommelhoff, *Nat. Phys.* **2023**, *19*, 1402.
[46] M. R. Bionta, F. Ritzkowsky, M. Turchetti, Y. Yang, D. Cattozzo Mor, W. Putnam, F. Kärtner, K. Berggren, P. Keathley, *Nat. Photonics* **2021**, *15*, 456.
[47] P. Dombi, Z. Pápa, J. Vogelsang, S. Yalunin, M. Sivis, G. Herink, S. Schäfer, P. Groß, C. Ropers, C. Lienau, *Rev. Mod. Phys.* **2020**, *92*, 025003.
[48] I. C. Benea-Chelmus, F. F. Settembrini, G. Scalari, J. Faist, *Nature* **2019**, *568*, 202.
[49] C. Riek, D. V. Seletskiy, A. S. Moskalenko, J. F. Schmidt, P. Krauspe, S. Eckart, S. Eggert, G. Burkard, A. Leitenstorfer, *Science* **2015**, *350*, 420.

© 2025 The Author(s). Laser & Photonics Reviews published by Wiley-VCH GmbH